

3D-ordered Nanoporous LiMPO₄ (M = Fe, Mn)–Carbon Composites with Excellent Charging–Discharging Rate-capability

Isamu Moriguchi,* Shohei Nabeyoshi, Mayato Izumi, and Hirotooshi Yamada
Graduate School of Engineering, Nagasaki University, 1-14 Bunkyo-machi, Nagasaki 852-8521

(Received September 19, 2012; CL-120978; E-mail: mrgch@nagasaki-u.ac.jp)

Highly ordered and three-dimensionally interconnected nanoporous materials, constructed with a nanothick wall of LiMPO₄ (M = Fe, Mn) and a carbon (C) nanocomposite, were successfully synthesized by a colloidal crystal-template process. It was demonstrated for the first time that the ordered nanoporous composites show excellent rate capability not only for LiFePO₄ but also for LiMnPO₄.

The recent progress in chemical fabrication of nanomaterials has prompted increased interest in nanoscale optimization of photo- and electrochemical functional materials, catalysts, and so on. Synthesis of Li-host nanoparticles is actually one of the recent research trends for yielding high-power Li-ion batteries.^{1–4} The down-sizing of Li-host materials is expected to shorten the Li-diffusion length in the solid phase to reduce Li insertion–extraction times. Olivine-type lithium metal phosphates have recently emerged as potential cathode materials for Li-ion batteries, because of their relatively high capacities and redox potentials, as well as their electrochemical stabilities. LiFePO₄ and LiMnPO₄ have particularly attracted a great deal of attention for their practical merits of low cost, natural abundance of Fe and Mn, and environmental benignity. However, these materials have inherently poor electronic conductivity and Li-ion diffusivity and hence poor rate-capability.⁵ Down-sizing of Li-host particles and their carbon coatings were effective in overcoming the latent problem for LiFePO₄^{3,5–9} but not enough for LiMnPO₄, having much lower conductivity than LiFePO₄.^{10–12} Since LiMnPO₄ theoretically has a higher energy density than LiFePO₄ because of its higher redox potential of 4.1 V vs. Li/Li⁺ (3.5 V for LiFePO₄), recent studies have focused on improving the charge–discharge properties of LiMnPO₄ by nanometer level structural control.^{4,13–17} It was reported that LiMnPO₄ nanocrystallites embedded in porous carbon show good rate capability as a result of an extension of the solid solution region in the LiMnPO₄ nanocrystallites, which lowers the kinetic barrier of the MnPO₄–LiMnPO₄ phase transition during Li insertion–extraction.¹⁸ Therefore, precise control of the nanocomposite structure composed of LiMnPO₄ and carbon is expected to bring about a high capacity and rate for LiMnPO₄-based materials.

Herein, we have newly developed ordered nanoporous materials with a three-dimensionally continuous nanothick wall composed of LiMPO₄ (M = Fe, Mn) and carbon. Such nanoporous composites are expected to provide a high surface area interface of electrolyte–active material for increasing the charge-transfer rate and active material nanophases in the nanothick wall for reducing the Li-diffusion length, as well as electron and ion conducting paths by way of carbon phases in the wall and nanopores, respectively.^{2,19,20} It is demonstrated for the first time that the ordered nanoporous composites show excellent rate-capability not only for LiFePO₄ but also for LiMnPO₄.

Nanoporous composites of LiMPO₄ (M = Fe, Mn) and carbon were synthesized by a polystyrene (PS) opal-template process as follows: A PS opal was obtained by centrifuging a monodispersed PS latex with a particle size of 190 nm (Seradyn Inc.) and subsequent drying in vacuo for 1 day. The opal was immersed for 5 days in an ethanol/water (20/80 by weight) mixed solution of LiNO₃, M(NO₃)₂·nH₂O (*n* = 4, 9 for M = Mn, Fe, respectively) and NH₄H₂PO₄, whose concentrations were adjusted to be 0.5 mol dm^{−3}. A small amount of nitric acid was added to the solution to dissolve inorganic sources completely for the LiMnPO₄ synthesis. The impregnated opal was dried in vacuo and was calcined in an Ar atmosphere at 700 °C for 16 h to yield a porous sample. To increase residual carbon content in the sample, an appropriate amount of sucrose was dissolved in the starting solution; its concentration was 0.16 mol dm^{−3} for LiFePO₄ and 1.0 mol dm^{−3} for LiMnPO₄. Hereafter, the porous samples are abbreviated as LFP-S(*x*) and LMP-S(*x*) for LiFePO₄ and LiMnPO₄, respectively, where *x* indicates the molar ratio of sucrose against the Fe or Mn atom in the starting solution. Nonporous samples, denoted as LFP[non] and LMP[non], were also synthesized without the PS opal by drying the starting solution and subsequent heating under the same conditions.

It was confirmed by XRD measurements that all the samples had a single crystalline phase of olivine LiMPO₄. Carbon content and BET surface areas of the samples are listed in Table 1. The samples obtained by the PS template process had higher BET surface area than the nontemplated for both LFP and LMP samples. The addition of sucrose in the starting inorganic solution increased the residual carbon content and BET surface area. As observed by SEM, an ordered nanoporous structure was successfully formed in LFP-S(*x*) powders in contrast to that of LFP[non], which was nonporous (Figures 1a and 1b). The pore sizes of LFP-S(*x*) were about 100 nm, corresponding to half of the PS particle diameter. Shrinkage of nanopores during the heat treatment would occur to form a conservative porous framework because the interstitial space of the PS opal was not filled with

Table 1. Structural characteristic of LFP and LMP samples

Samples	Surface area /m ² g ^{−1} ^a	Carbon content /wt % ^b
LFP[non]	9	n.d.
LFP-S(0)	58	6.9
LFP-S(0.32)	132	14.7
LMP[non]	10	n.d.
LMP-S(0)	49	1.6
LMP-S(2)	124	25.0

^aDetermined by the Brunauer–Emmett–Teller (BET) method from N₂ adsorption isotherms. ^bDetermined by elementary analysis.

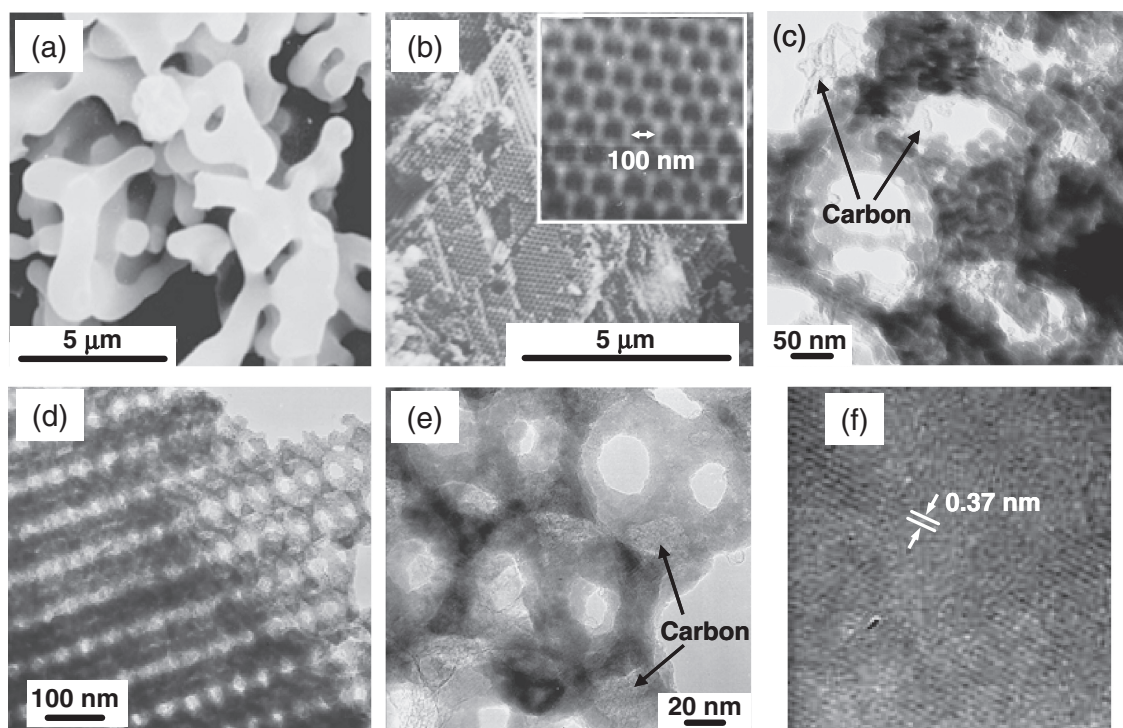


Figure 1. (a) SEM image of LFP[non], (b) SEM image of LFP-S(0), (c) TEM image of LFP-S(0), (d) TEM image of LFP-S(0.32), (e) enlarged image of a part of (d), and (f) a crystallite phase in pore wall in (e).

only inorganic solid for the present synthetic procedure using the inorganic solution. It can be seen by TEM that the pore wall of LFP-S(0) was constructed with LiFePO_4 nanocrystallites and residual carbon deposited rather heterogeneously on the surfaces of nanopore walls (Figure 1c). The sizes of the LiFePO_4 nanocrystallites, which were observed by TEM to be ca. 30 nm, are comparable to the primary crystallite size estimated from the full width at half-maximum (FWHM) of the XRD peaks using the Scherrer equation. Conversely, LFP-S(0.32) possessed a highly ordered nanoporous structure with a pore size of ca. 80 nm and a wall thickness of ca. 25 nm (Figure 1d). As shown in Figure 1e, the pore wall was constructed with amorphous carbon and LiFePO_4 nanocrystallites; Figure 1f shows one of the crystalline phases, and the line distance of 0.37 nm corresponds to the (010) plane spacing of LiFePO_4 . The residual carbon was deposited not only on the surface of the nanopores but also inside the pore wall for LFP-S(0.32). The incorporation of residual carbon into the wall is considered to cause high ordering of the nanoporous structure for LFP-S(0.32), and hence the BET surface area of LFP-S(0.32) was about twice as large as that of LFP-S(0), in spite of a small excess amount of residual carbon. Such an ordered macroporous structure was also successfully formed for the LMP-S(x) samples (Figure 2). LMP-S(2), having a higher carbon content and BET surface area than LMP-S(0), showed a three-dimensionally interconnected porous structure throughout.

Figures 3a and 3b show charge–discharge curves measured by means of the constant-current (CC) mode for LFP samples and the CC and subsequent constant–voltage (CC–CV) mode for LMP samples. All the LFP and LMP samples exhibited typical potential plateaus at around 3.4 and 4.0 V vs. Li/Li^+ in

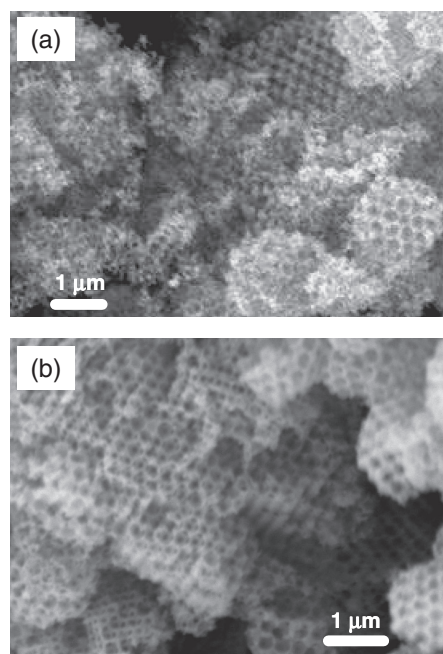


Figure 2. SEM images of (a) LMP-S(0) and (b) LMP-S(2).

discharge curves, respectively, which are related to the phase transition of FePO_4 – LiFePO_4 and MnPO_4 – LiMnPO_4 as reported already.²¹ The porous samples showed extended plateaus and much larger charging–discharging capacities than the nontemplated. Further increases in the capacities were observed on porous samples with higher carbon contents. LMP-S(2) showed

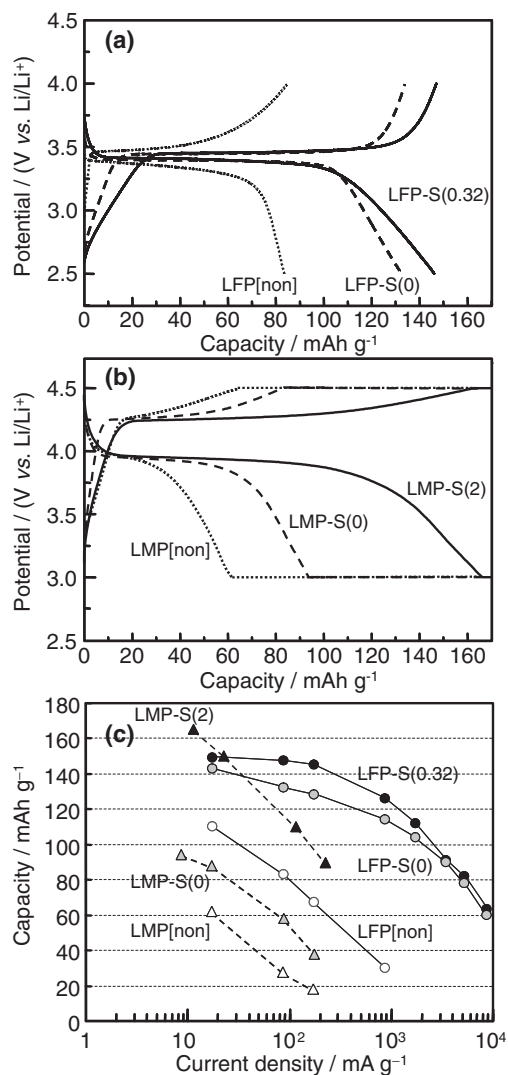


Figure 3. (a) CC curves of LFP samples at the constant current of 17 mA g^{-1} (0.1 C), (b) CC-CV curves of LMP samples at $10\text{--}21 \text{ mA g}^{-1}$: 17 mA g^{-1} for LMP[non], 10 mA g^{-1} for LMP-S(0), 21 mA g^{-1} for LMP-S(2), and (c) rate capability of LFP and LMP samples.

a reversible capacity of 167 mA h g^{-1} at $C/20$ ($1 \text{ C} = 171 \text{ mA h g}^{-1}$), which is very close to the theoretical limitation (171 mA h g^{-1}). These results indicate that the nanoporous composite structure consisting of olivine nanocrystallites and carbon residue is effective in yielding high capacity, even for highly insulating LiMnPO_4 .

The porous composite samples were obviously superior in rate capability to the nonporous samples, as shown in Figure 3c. Specifically, LFP-S(0.32) had very high capacities at high rates of 126 mA h g^{-1} at 5 C and 112 mA h g^{-1} at 10 C ($1 \text{ C} = 170 \text{ mA h g}^{-1}$), which are comparable to the best performance reported on carbon-coated LFP nanoparticles without Fe_2P , if compared in the same potential range.¹⁰ However, LMP-S(2) showed the best rate capability among the reported LiMnPO_4 , to the best of our knowledge: 115 mA h g^{-1} at 1 C, 90 mA h g^{-1} at 2 C in the potential range $4.5\text{--}3.0 \text{ V}$ vs. Li/Li^+ at room

temperature. It was also confirmed that the nanoporous composites showed good cycling performance; for example, the capacity of LFP-S(0.32) was maintained even after 100-cycle full charging–discharging at 5 C.

In conclusion, this study represents the first example of 3D-ordered nanoporous materials constructed with a nanothick wall of LiMPO_4 –carbon nanocomposites, which show high rate charging–discharging properties, even for highly insulating LiMnPO_4 . Although the nanoporous LiMnPO_4 –C is still inferior to the nanoporous LiFePO_4 –C in rate capability at present, this will be resolved by optimizing the structural parameters such as pore size, wall thickness, and composition through further investigations.

The study made use of XRD in the Center for Instruments Analysis of Nagasaki University. This work was partly supported by a Grant-in-Aid for Scientific Research from Ministry of Education, Culture, Sports, Science and Technology of Japan.

References

- 1 M. Okubo, Y. Mizuno, H. Yamada, J. Kim, E. Hosono, H. Zhou, T. Kudo, I. Honma, *ACS Nano* **2010**, *4*, 741.
- 2 I. Moriguchi, R. Hidaka, H. Yamada, T. Kudo, H. Murakami, N. Nakashima, *Adv. Mater.* **2006**, *18*, 69.
- 3 D.-H. Kim, J. Kim, *Electrochem. Solid-State Lett.* **2006**, *9*, A439.
- 4 D. Choi, D. Wang, I.-T. Bae, J. Xiao, Z. Nie, W. Wang, V. V. Viswanathan, Y. J. Lee, J.-G. Zhang, G. L. Graff, Z. Yang, J. Liu, *Nano Lett.* **2010**, *10*, 2799.
- 5 C. Delacourt, L. Laffont, R. Bouchet, C. Wurm, J.-B. Leriche, M. Morcrette, J.-M. Tarascon, C. Masquelier, *J. Electrochem. Soc.* **2005**, *152*, A913.
- 6 B. Kang, G. Ceder, *Nature* **2009**, *458*, 190.
- 7 P. Gibot, M. Casas-Cabanas, L. Laffont, S. Levasseur, P. Carlach, S. Hamelet, J.-M. Tarascon, C. Masquelier, *Nat. Mater.* **2008**, *7*, 741.
- 8 Y.-H. Huang, K.-S. Park, J. B. Goodenough, *J. Electrochem. Soc.* **2006**, *153*, A2282.
- 9 K. Striebel, J. Shim, A. Sierra, H. Yang, X. Song, R. Kostecki, K. McCarthy, *J. Power Sources* **2005**, *146*, 33.
- 10 Y. Wang, J. Wang, J. Yang, Y. Nuli, *Adv. Funct. Mater.* **2006**, *16*, 2135.
- 11 T. Drezen, N.-H. Kwon, P. Bowen, I. Teerlinck, M. Isono, I. Exnar, *J. Power Sources* **2007**, *174*, 949.
- 12 N. N. Bramnik, H. Ehrenberg, *J. Alloys Compd.* **2008**, *464*, 259.
- 13 S. Aono, K. Urita, H. Yamada, I. Moriguchi, *Chem. Lett.* **2012**, *41*, 162.
- 14 D. Wang, H. Buqa, M. Crouzet, G. Deghenghi, T. Drezen, I. Exnar, N.-H. Kwon, J. H. Miners, L. Poletto, M. Grätzel, *J. Power Sources* **2009**, *189*, 624.
- 15 S.-M. Oh, S.-W. Oh, C.-S. Yoon, B. Scrosati, K. Amine, Y.-K. Sun, *Adv. Funct. Mater.* **2010**, *20*, 3260.
- 16 J. Ni, Y. Kawabe, M. Morishita, M. Watada, T. Sakai, *J. Power Sources* **2011**, *196*, 8104.
- 17 F. Wang, J. Yang, P. Gao, Y. NuLi, J. Wang, *J. Power Sources* **2011**, *196*, 10258.
- 18 S. Aono, K. Urita, H. Yamada, I. Moriguchi, *Solid State Ionics*, **2012**, *225*, 556.
- 19 I. Moriguchi, F. Nakahara, H. Furukawa, H. Yamada, T. Kudo, *Electrochem. Solid-State Lett.* **2004**, *7*, A221.
- 20 H. Yamada, H. Nakamura, F. Nakahara, I. Moriguchi, T. Kudo, *J. Phys. Chem. C* **2007**, *111*, 227.
- 21 M. Yonemura, A. Yamada, Y. Takei, N. Sonoyama, R. Kanno, *J. Electrochem. Soc.* **2004**, *151*, A1352.